



Original research article

The establishment of the anther somatic niche with single-cell sequencing

D. Blaine Marchant ^{a,b,*}, Virginia Walbot ^{b,**}^a Department of Biology, University of Missouri – St. Louis, St. Louis, MO, 63121, USA^b Department of Biology, Stanford University, Stanford, CA, 94305, USA

A B S T R A C T

The anther is the developmental housing of pollen and therefore the male gametes of flowering plants. The meiotic cells from which pollen are derived must differentiate *de novo* from somatic anther cells and synchronously develop with the rest of the anther. Anthropogenic control over another development has become crucial for global agriculture so as to maintain inbred lines and generate hybrid seeds of many crops. Understanding the genes that underlie the proper differentiation, developmental landmarks, and functions of each anther cell type is thus fundamental to both basic and applied plant sciences. We investigated the development of the somatic niche of the maize (*Zea mays*) anther using single-cell RNA-seq (scRNA-seq). Extensive background knowledge on the birth then pace and pattern of cell division of the maize anther cell types and published examples of cell-type gene expression from *in situ* hybridization allowed us to identify the primary cell types within the anther lobe, as well as the connective cells between the four lobes. We established the developmental trajectories of somatic cell types from pre-meiosis to post-meiosis, identified putative marker genes for the somatic cell types that previously lacked any known specific functions, and addressed the possibility that tapetal cells sequentially differentiate. This comprehensive scRNA-seq dataset of the somatic niche of the maize anther will serve as a baseline for future analyses investigating male-sterile genotypes and the impact of environmental conditions on male fertility in flowering plants.

1. Introduction

Pollen is essential for sexual reproduction in flowering plants as it is the housing and means of transportation for male gametes. While animals typically establish germlines for gamete production in their embryos, plants lack such predetermined pre-meiotic cell lineages. Instead, plants have pluripotent meristems that develop continuously into vegetative (leaf, stem, root) and later into reproductive (floral) tissues. The stamen is the male reproductive organ of a flower and consists of an anther and filament (Fig. 1). Analogous to the mammalian testis, the anther is where pollen and the male gametes develop; however, the meiotic cells from which pollen are derived must differentiate *de novo* from somatic anther cells and synchronously develop with the rest of the anther. The finely choreographed differentiation of each anther cell layer is essential for pollen production and, therefore, male fertility in flowering plants. Anthropogenic control over the timing, environmental triggers, quantity, and overall competence of anther development has become crucial for global agriculture so as to maintain inbred lines and generate hybrid seeds of many crops. Even in natural plant systems, international concern over the effects of climate change on pollen production has ballooned in the last decade, because pollen development is an acutely environmentally sensitive process (De Strome and Geelen, 2014; Santiago and Sharkey, 2019). A single day of extreme heat or cold

can delay or disrupt pollen development, essentially sterilizing the plants (Barnabás et al., 2008). Understanding the genes that underlie the proper differentiation, developmental landmarks, and functions of each anther cell type is thus fundamental to both basic and applied plant sciences.

A mature anther consists of four lobes centrally linked by connective and vascular tissue to form a butterfly-like shape when viewed transversely (Fig. 1B). The somatic cell types of the anther lobe are well-conserved across flowering plants and consist of four cell types: the epidermis, endothecium, middle layer, and tapetum. Anther lobes exhibit a dartboard architecture; each somatic cell type typically forms a single cell layer encircling the central germinal cells (Fig. 1B). We reported single-cell RNA-seq (scRNA-seq) analyses of the maize germinal lineage from pre-meiotic archesporial cells to pollen to define the developmental trajectory, pinpoint episodes of rapid transcriptome change, and to resolve when haploid gene expression begins after meiosis (Nelms and Walbot, 2019, 2022). While the origin and development of the somatic anther cell types have been described through microscopy and genetic analyses largely focused on male-sterile genotypes with one or more defective cell types (Gómez et al., 2015; Marchant and Walbot, 2022; Verma, 2019), few cell-type specific analyses are available for anther somatic cell types (Li et al., 2017, 2024; Long et al., 2021; Zhou et al., 2022).

* Corresponding author. Department of Biology, University of Missouri – St. Louis, St. Louis, MO, 63121, USA.

** Corresponding author.

E-mail addresses: dbmarchant@umsl.edu (D.B. Marchant), walbot@stanford.edu (V. Walbot).

In this study, we investigated the development of the somatic niche of the maize (*Zea mays*) anther using scRNA-seq. Maize has been used as a model system for studying anthers for decades in part, because high productivity of this major agricultural crop for nearly 100 years has relied on hybrid seed, requiring control of pollen distribution to insure cross-pollination between two inbred parents. Maize is monoecious, with separate male and female inflorescences (tassel and ear, respectively). The tassel is comprised of hundreds of male-only spikelets, each spikelet encompassing an upper and lower floret. Each floret contains three developmentally synchronous anthers; however, the upper-floret anthers are about one day more advanced in development. In addition, spikelet development varies by location along the main spike and side branches of the tassel (Egger and Walbot, 2015), allowing the dissection and isolation of anthers that span about 7 days of developmental stages from a single tassel; developmental stage can be charted by anther length (Fig. 1C). In the maize inbred line W23, anther development requires 30 days: starting from a few cells in each of the four lobes, then within five days all cell types are specified and the populations expand mitotically to reach nearly full cell number of 50,000 cells by day 15 (mid-meiosis) (Kelliher and Walbot, 2011).

These favorable anatomical features and extensive background knowledge on the birth then pace and pattern of cell division of the maize anther cell types and published examples of cell-type gene expression from *in situ* hybridization allowed us to identify the primary cell types within the anther lobe, as well as the connective cells between the four lobes. We established the developmental trajectories of somatic

cell types from pre-meiosis to post-meiosis, identified putative marker genes for the somatic cell types that previously lacked any known specific functions, addressed the possibility that tapetal cells sequentially differentiate, and interrogated middle layer cells for evidence of programmed cell death markers. This comprehensive scRNA-seq dataset of the somatic niche of the maize anther will serve as a baseline for future analyses investigating male-sterile genotypes and the impact of environmental conditions on male fertility in flowering plants.

2. Results

2.1. Identification of maize anther cell types

We quantitatively released, isolated, and sequenced individual fixed cells from maize anthers spanning 0.5 mm–3.0 mm in length by increments of 0.25 mm. Temporally, the initial stages in this series are approximately one day apart, but after the 1.75 mm stage, the samples are closer to 2 days apart. This developmental series spans the stage prior to division of the secondary parietal layer (SPL) into both the tapetum and middle layer thus finalizing establishment of each of the somatic cell layers all the way to the impending programmed cell death of the tapetum. In total, 2182 cells met our quality thresholds after the removal of cell cycle-regulated genes (Nelms and Walbot, 2019). Overall, transcripts from 22,173 distinct genes were detected, similar to the diversity of gene expression documented in whole anther RNA-seq analyses (Nan et al., 2022; 2017; Zhou et al., 2022). We compared the

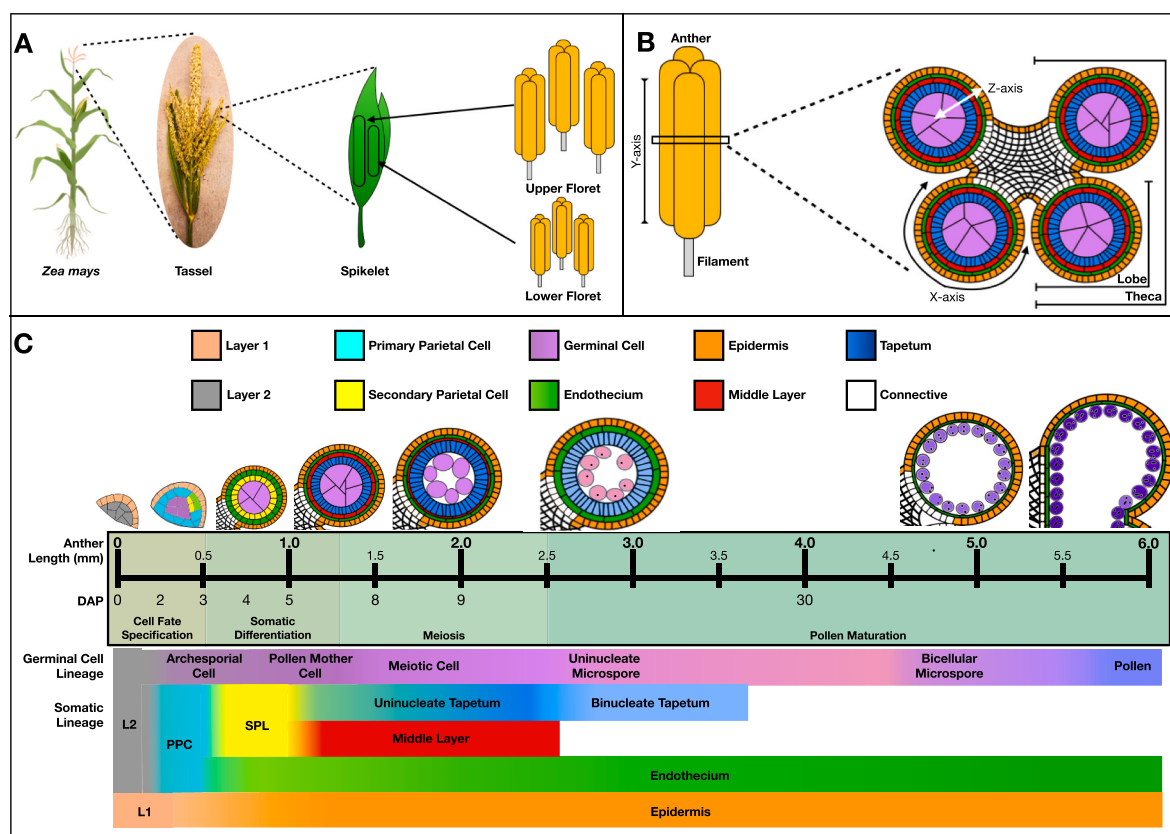


Fig. 1. Maize anther anatomy and development. (A) The maize tassel is the apical male-only inflorescence containing hundreds of spikelets. A spikelet has an upper and lower floret each with three developmentally synchronous anthers. The upper-floret anthers are about one day more advanced in development than the lower-floret anthers. (B) On the left is a schematic of a 2.0 mm anther and filament. In the right transverse view, the 2.0 mm anther is composed of four lobes each containing the four somatic cell types and germinal cells. The four lobes can be divided into two theca, each of which consists of an abaxial and an adaxial lobe. In the central diagram the X axis (circumferential around each lobe) and the Z axis (transverse across a lobe) are indicated. (C) Across the top of the diagram, the sequential stages of anther development are displayed in cartoons relative to anther length (mm), days after primordia initiation, and successive major developmental stages. Developmental progression is highly regular, such that anther length is a reasonable guide to the stage of cell development within the anther. Below the staging system, there is a schematic representation of the emergence of cell types.

transcript diversity of previously published whole 2.0 mm maize anther RNA-seq data to the transcript diversity across all our 2.0 mm cells. In total, 90% of the scRNA-seq transcribed genes were also found to be transcribed in the whole anther RNA-seq dataset.

We expected seven cell clusters representing vascular, connective, germinal, tapetal, middle layer, endothelial, and epidermal cell types; however, we identified ten distinct clusters of cells (Fig. 2). Anther stage clearly influenced cell clustering as some of the clusters were biased in composition by anther stage (Fig. 2B, Suppl. Fig. 1). Using previously validated anther marker genes, the known biological functions of specific anther cell types, and the anther stage composition, we were able to

readily identify six of the ten clusters.

Clusters 1 and 2 were almost completely comprised of cells from ≥0.75 mm anthers. Notably, both the epidermis and endothecium are established early in anther development and persist throughout (Fig. 1C). Cuticular waxes are synthesized in the epidermis and used to protect the anther from biotic and abiotic factors. Expression of the maize homolog of the rice *WAX-DEFICIENT ANTERI* (*WDA1*), the knock-out of which has a significantly reduced epicuticular load (Jung et al., 2006), was specifically enriched in Cluster 1 identifying this cluster as the epidermis (Fig. 2C). Chloroplasts are a unique characteristic of the endothecium (Murphy et al., 2015; Zhu et al., 2020),

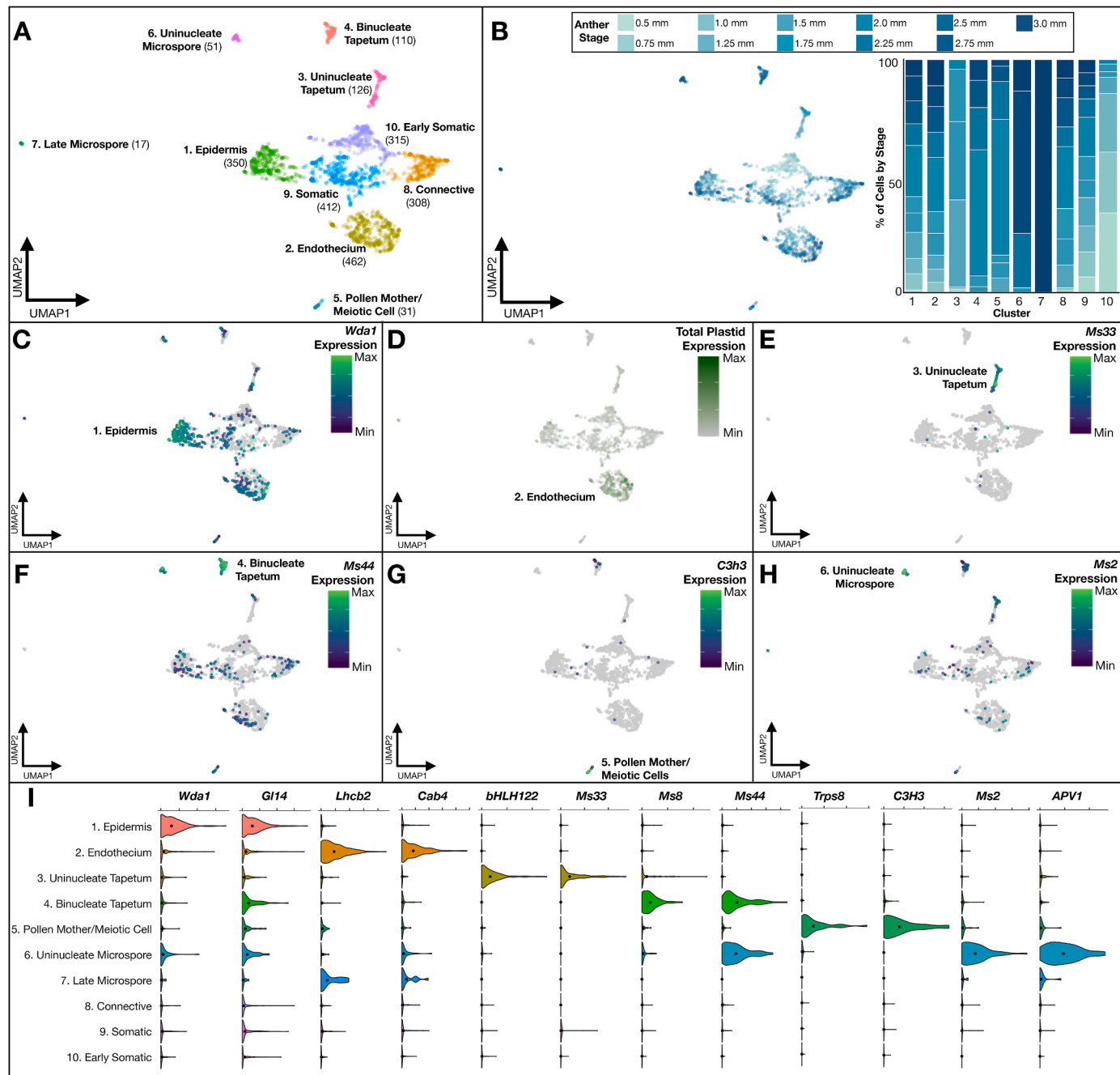


Fig. 2. Identification of maize anther cell types. (A) Uniform Manifold Approximation and Projection (UMAP) of maize anther cells categorized into ten distinct clusters and their putative cell types. The number of cells per cluster are in parentheses. (B) UMAP of maize anther cells by anther stage and percentage of cells by anther stage per cluster. (C–H) UMAPs of previously identified marker gene expression for the maize anther epidermis (C), endothecium (D), uninucleate tapetum (E), binucleate tapetum (F), pollen mother/meiotic cells (G), and uninucleate microspores (H). (I) Violin plots of known marker gene expression values for specific maize anther cell types by cluster.

therefore we used the percentage of plastid transcripts per cell as the primary indicator of this cell type (Suppl. Fig. 2). Cluster 2 was highly enriched for plastid transcripts identifying it as the endothecium (Fig. 2D).

The majority of cells in Cluster 3 were from 1.25 to 1.75 mm anthers and the older 2.0–2.75 mm anthers constituted Cluster 4. *MALE-STERILE33* (*MS33*) identified Cluster 3 as uninucleate tapetum, because *MS33*

expression is known to be enriched in the tapetum during meiosis (Zhang et al., 2018) (Fig. 2E). Cluster 4 was identified as binucleate tapetum by the enrichment of *MALE-STERILE44* (*MS44*) expression (Fig. 2F), a known marker gene for the tapetum at the end of meiosis continuing into the uninucleate microspore stage of anther development (Fox et al., 2017).

The cells in Cluster 5 were largely from 2.0 mm anthers and 2.25–3.0

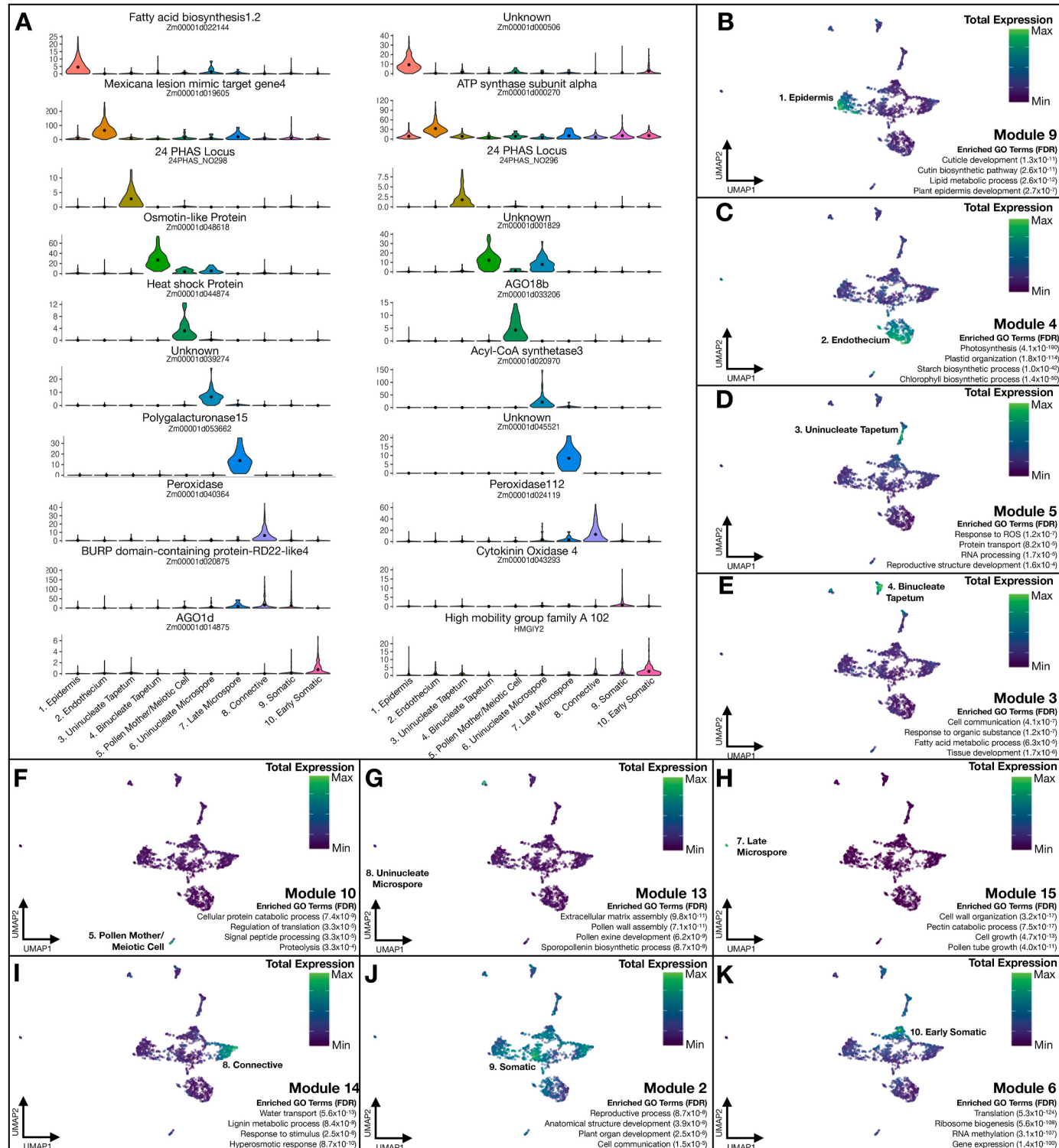


Fig. 3. *De novo* marker genes and biological function of enriched co-regulated gene modules. (A) Violin plots of the expression values for the top two *de novo* marker genes and annotations for each maize anther cell type. (B–K) UMAPs of the aggregated expression of co-regulated genes specifically enriched in each anther cell type along with four select significantly ($p < 0.05$) enriched gene ontology (GO) terms and associated false discovery rate (FDR) values.

mm for the cells of Cluster 6. These two distinct clusters were readily identified as germinal cells by the marker genes *C3H TRANSCRIPTION FACTOR33* (*C3H3*) and *MALE-STERILE2* (*MS2*) (Nelms and Walbot, 2019; Xu et al., 2021), representing the pre-meiotic pollen mother/meiotic cells (Cluster 5) and post-meiosis, early uninucleate microspores (Cluster 6) (Fig. 2G–H). We further confirmed the identity of these six clusters via secondary marker genes (Fig. 2I–Suppl. Table 1).

Differentially expressed (DE) genes were identified for each cluster (Fig. 3, Suppl. Table 2). A subset of these genes confirmed our identification of the six known clusters based on their annotations, pathways, and homology to well-studied genes in other plants. A gene involved in fatty-acid biosynthesis was one of the top DE genes in the epidermis (Zhang et al., 2019). Similarly, the top two endothecium DE genes were chloroplastic, while two 24-nucleotide phased small interfering RNA loci (24-PHAS loci), which are known to be up-regulated in the tapetum during prophase I of meiosis (1.25–1.5 mm) (Nan et al., 2022; Zhou et al., 2022), were the top DE genes for the uninucleate tapetum. Laser-capture microdissection of maize anther cell types previously identified both *ARGONAUTE18B* (*AGO18B*) and the small heat shock protein (sHSP) gene Zm00001d044874 as highly enriched in the pollen mother cells (Zhou et al., 2022), both of which were the top DE genes for the pollen mother/meiotic cells cluster in this scRNA-seq dataset.

Particularly informative were the DE genes for the unidentified clusters. One of the DE genes for Cluster 7, the gene encoding a polygalacturonase (*ZmPG15*), was previously found to be highly expressed in stage 11 (late uninucleate microspore stage) anthers (Lu et al., 2021). Although the cell type specificity of this gene is currently unestablished, the paucity of cells in Cluster 7 could reflect the low relative abundance of germinal cells (<1% of total cells) in maize anthers (Kelliher and Walbot, 2011). The fact that all of the cells in Cluster 7 are from 3.0 mm anthers and the sizeable distance of Cluster 7 to the other clusters suggests these to be late uninucleate microspores.

The identity of Cluster 8 was also unknown, however, we found two peroxidase genes to be the top DE genes for this cluster. Peroxidases (PRX) are essential for lignification and the polymerization of plant cell wall elements (Fernández-Pérez et al., 2015; Shigeto et al., 2015), suggesting Cluster 8 could be the connective cells, through which the anther draws nutrients from the rest of the plant. Examining the most highly enriched genes was not helpful for either Clusters 9 or 10, as the expression of the DE genes for Cluster 9 were highly variable among its cells and *AGO1d*, the DE gene for Cluster 10, is known to be expressed across all the somatic cell types before and during meiosis (Shi et al., 2022; Zhou et al., 2022).

Considerable insight can be gained into the clusters by investigating the biological functions of their specifically enriched genes. We identified modules of co-regulated genes specific to each cluster then analyzed the gene ontology (GO) term enrichment for each of the cluster-specific modules (Suppl. Fig. 3, Suppl. Tables 3–4). These analyses validated our identification of the epidermis, endothecium, uninucleate tapetum, binucleate tapetum, pollen mother/meiotic cells, and uninucleate microspores based on the significant enrichment of concurrent GO terms and the known biology of these cell types (Fig. 3B–G). The GO term analysis of Module 15, which was highly enriched in Cluster 7, further supports the identification of these cells as late uninucleate microspores as genes associated with cell wall organization, cell growth, and pollen tube development were all significantly enriched (Fig. 3H). Similarly, Module 14 was enriched for genes associated with water transport, stimulus response, lignification, and hyperosmotic response, all functions expected of the connective cells in Cluster 8 (Fig. 3I).

We next asked if the SPL cells, precursors to both the middle layer and tapetum, and the derivative middle layer cells were identifiable in the dataset. There are no published marker genes for these cell types, however, the SPL cells should be present in 0.5 mm anthers, and less abundant at 0.75 mm, a day later, as most SPL cells will have divided periclinally to generate middle layer and tapetal cells. Module 2, which was enriched in Cluster 9, yielded vague but significant GO terms

associated with plant anther development (Fig. 3J). The cells of Cluster 10 were extremely (FDR <1.0x10⁻¹⁰⁰) enriched for genes associated with transcription and translation based on Module 6 (Fig. 3K). The lack of early (≤ 1.0 mm) cells in the tapetal clusters, proximity to the uninucleate tapetal cluster, and composition of young (≤ 1.25 mm) cells suggests Cluster 10 contains SPL cells, young tapetal cells, and likely middle layers cells that have not yet acquired cell-type specific gene expression. Therefore, we categorized Cluster 10 as early somatic cells, likely a mixed population of the precursor SPL and daughter derivatives (middle layer and tapetum), and Cluster 9 as unknown somatic cells for which no clear genes were recovered.

2.2. Development of the somatic niche in maize anthers

We next analyzed the developmental trajectories for each of the established cell types. By isolating the tapetal, endothelial, epidermal, germinal, and connective cells from our dataset, we investigated their transcriptional changes across the developmental series. Combining the uninucleate and binucleate tapetum cells, we found the tapetum underwent the most pronounced transcriptional changes, notably at the 1.75–2.0 mm transition (Fig. 4). The activation of nine genes, including Zm00001d048618, and the deactivation of eight genes, including 24-PHAS_NO180, specify the 1.75–2.0 mm differentiation point (Fig. 4B). Prior analysis of maize anther development established that more than 100 24-PHAS loci are abruptly down-regulated by 2.0 mm (Zhai et al., 2015). These prominent transcriptomic changes are further illustrated by the significant gap in pseudotime between stages, defining the variation between the uninucleate and binucleate tapetum (Fig. 4C). Other genes were less discrete in their expression across the developmental trajectory of the tapetum, such as Zm00001d031168 which gradually increased in expression across the developmental stages. The scarcity of clearly defined early (≤ 1.25 mm) tapetal cells hinders our ability to analyze the establishment of this cell type, however, the initial peak and drop of pseudotime velocity suggests major transcriptomic rearrangement early in tapetal development.

In contrast, analysis of the epidermis indicated virtually no peaks in pseudotime velocity beyond the beginning and end of the developmental series (Fig. 4A). A select few genes were gradually activated over the development of the epidermis; however, most were relatively static in expression (Suppl. Fig. 4B). The endothecium displayed multiple changes in pseudotime velocity early in development but was otherwise static in its transcriptomic profile (Suppl. Fig. 4A). Although plastids are prominent and starch accumulates in the endothecium from the earliest stages, the plastids differentiate as chloroplasts after perceiving light, which is required for chlorophyll synthesis, after the 1.0 mm stage (Murphy et al., 2015); later in development these chloroplasts are photosynthetically active (Zhu et al., 2020). The developmental trajectory of the connective cells was also relatively static with virtually no peaks in pseudotime velocity across our developmental series (Suppl. Fig. 4C). Similar to the results from Nelms and Walbot (2019, 2022), the germinal cell lineage clearly displayed major differentiation events throughout its development (Suppl. Fig. 4D). The two most dominant peaks were at 2.25 mm and at 3.0 mm, likely corresponding with the major differentiation points during meiosis and late uninucleate microspore development identified by Nelms and Walbot (2022).

2.3. Cell-cycle gene expression across maize anther cell types

All cell-cycle genes were removed during the initial analysis of maize anther cells as they are known to distort the clustering of scRNA-seq datasets, however, we questioned whether specific cell types were undergoing cell division more often than others as documented by Kelliher and Walbot (2011). Mapping the transcripts from this cohort of 456 genes back onto our individual cells, we quantified the overall expression of the cell-cycle regulated genes and their respective categories (Nelms and Walbot, 2019). Interestingly, the cell-cycle genes were

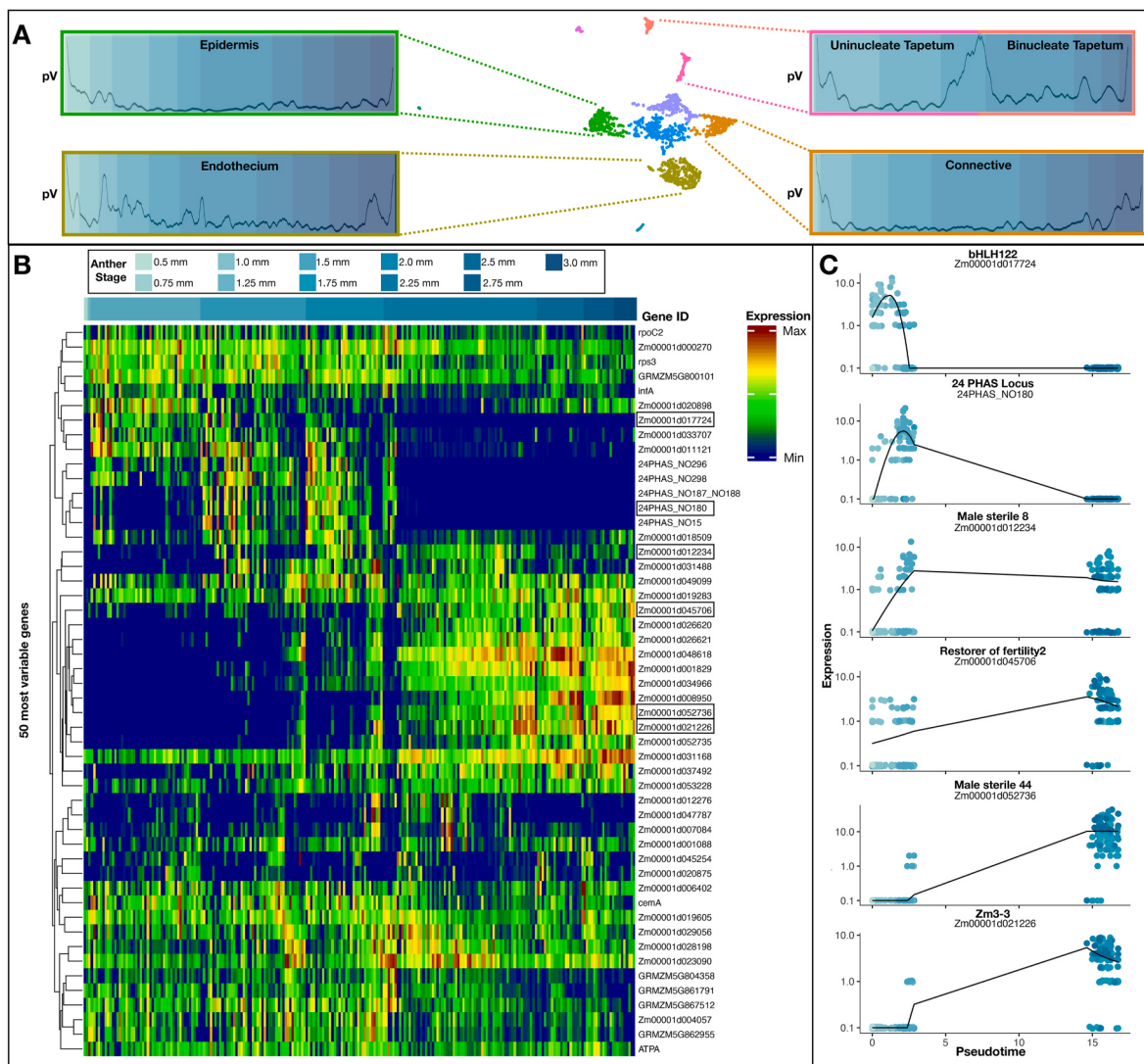


Fig. 4. Development and differentiation of the tapetum. (A) Pseudotime velocities across development for the epidermis, endothecium, tapetum, and connective cells. (B) Expression profile for the 50 most variable genes across 236 uninucleate and binucleate tapetal cells (Clusters 3 and 4), ordered by anther stage and pseudotime within each stage. (C) Expression values of select genes in tapetal cells over pseudotime.

relatively few when averaged across all cells, comprising only 3.3% of total transcripts per cell on average. Yet, when examining the expression clustering and outliers of each cell type, a more nuanced story emerges. The expression of Cell Growth 1 (G1) genes was largely ubiquitous across the ten clusters, with relatively low (~1%) but invariable expression (Fig. 5A). In contrast, cells undergoing the transition into DNA synthesis (G1/S genes) were much more variable, displaying sub-cluster localization in all of the clusters with the exception of the late microspores (Fig. 5B). The unknown somatic cells (Cluster 9) was significantly enriched for G1/S transcripts relative to the other clusters. A similar but more extreme pattern was found in purely DNA synthesis genes (S genes) with extreme outliers in all but the germinal cells, reaching >10% of S transcripts, and the unknown somatic cells having overall more S transcripts than any other cluster (Fig. 5C). Genes associated with the Cell Growth 2 (G2) stage and start of mitosis (G2/M) also displayed sub-cluster localization and extreme outliers predominantly in the two unidentified somatic clusters and connective cells (Fig. 5D). Mitotic (M) transcripts had the most clearly defined sub-clusters, notably in the unknown somatic cell cluster spanning towards the connective cells and early somatic cells (Fig. 5E). When all of the cell-cycle transcripts are summed, it is evident that cells in the somatic and early somatic cell clusters (Clusters 9 and 10) are undergoing significantly

more cell divisions than the other cell types. This fits well with the proposed composition of SPL, middle layer, and immature tapetal cells. Cell counts established that all three of these cell types exhibit the highest frequency of cell division, as does 5-ethynyl-2'-deoxyuridine (EdU) labeling of DNA synthesis during anther development (Egger and Walbot, 2016; Kelliher and Walbot, 2011). Therefore, we conclude that early somatic cells consist of the rapidly dividing SPL, middle layer, and tapetal cells up to the 1.0 mm stage, and somatic cells, composed of later stage cells, is also a mixture of still dividing cell types including tapetal cells that have not yet expressed typical marker genes.

It is also noteworthy that endothelial cells (Cluster 2) also express genes from all cell cycle stages. Endothelial cells are only 5–7 µm in the longitudinal direction, and as the anther grows in length, cell division rather than cell expansion occurs in the endothecium (Kelliher and Walbot, 2011). Cell division therefore continues throughout the period examined here.

3. Discussion

The germinal cell lineage is often the primary focus in plant reproduction and anther studies as it is the source of pollen and male gametes (Kelliher and Walbot, 2012; Nelms and Walbot, 2019, 2022; Wang et al.,

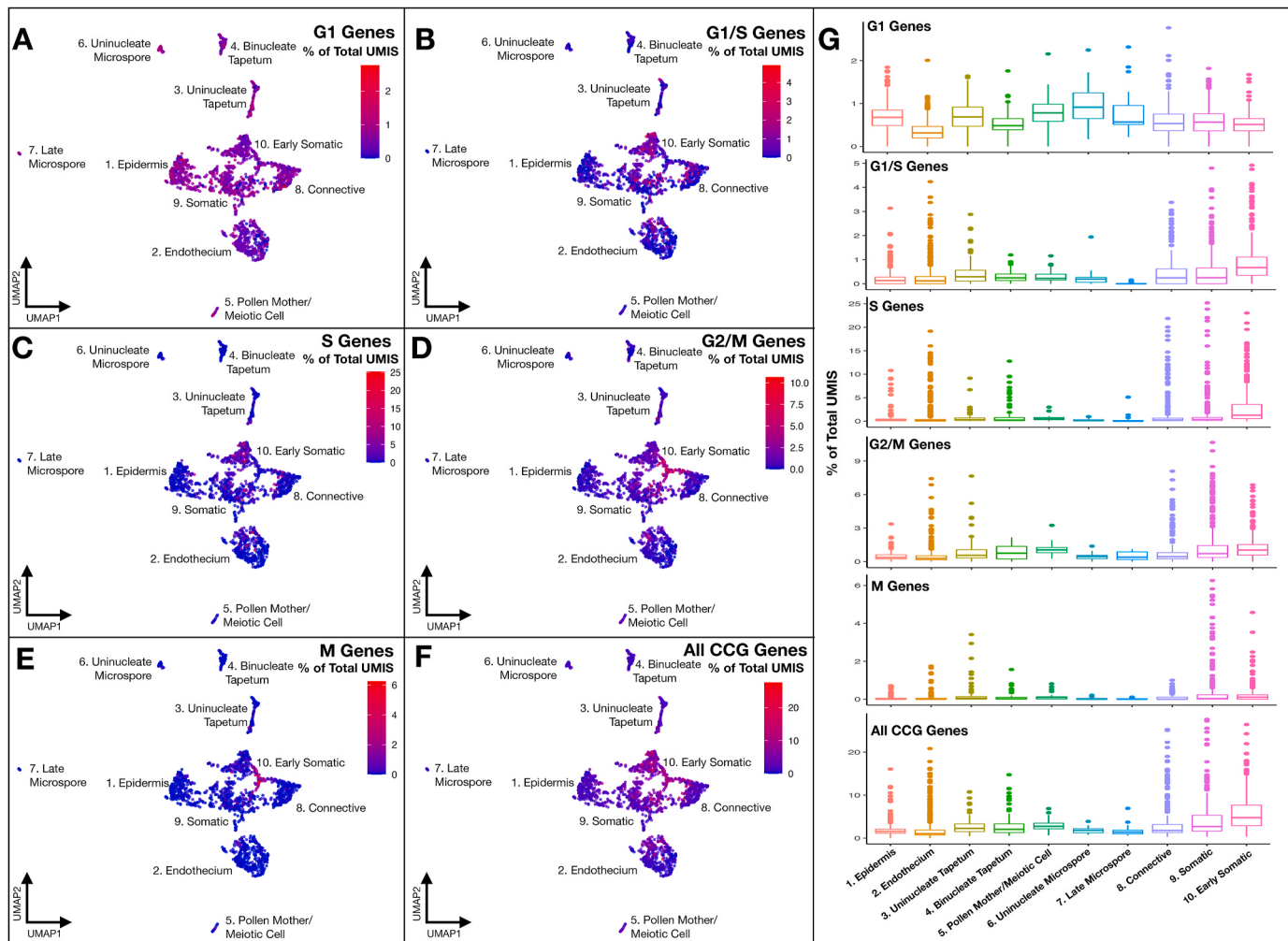


Fig. 5. Cell cycle-regulated gene expression by anther cell type. (A) UMAP of the percentage of total transcripts that are mapped to G1 related genes for each cell. (B) UMAP of the percentage of total transcripts that are mapped to G1/S related genes for each cell. (C) UMAP of the percentage of total transcripts that are mapped to S related genes for each cell. (D) UMAP of the percentage of total transcripts that are mapped to G2/M related genes for each cell. (E) UMAP of the percentage of total transcripts that are mapped to M related genes for each cell. (F) UMAP of the percentage of total transcripts that are mapped to all cell cycle-regulated genes for each cell. (G) Boxplots of the percentage of total transcripts that are mapped to G1, G1/S, S, G2/M, M, and all cell cycle-regulated genes by cluster. The horizontal lines within the box plots represent the median value, the lower and upper bounds of the box plots represent the first and third quartiles, whiskers extend to 1.5x the interquartile range, and all other points are outliers.

2012). And yet, numerous studies of male-sterile mutants have established that male fertility requires proper development of the somatic cell types housing the meiocytes before and during meiosis (reviewed in (Cheng et al., 1979; Kelliher et al., 2014; Marchant and Walbot, 2022; Walbot and Egger, 2016; Wiese et al., 2024)). Here, we identified cells from each of the somatic cell types in the maize anther lobe and the central connective cells and produced a developmental progression for each, defining the points of major and minor transcriptomic changes and functional roles before, during, and after meiosis.

The tapetum is well-investigated as it is the nutritive “nurse” cell layer directly surrounding the germinal cells and because the majority of male-sterile mutants exhibit tapetal defects (Skibbe et al., 2008; van der Linde and Walbot, 2019). The tapetum has six primary roles in anther development: 1) provide nutrients to the germinal cells; 2) secrete β -glucanase at the beginning of meiosis to remodel excess callose surrounding the meiocytes and again at the end of meiosis to dissolve the callose encasing each tetrad to release the individual haploid microspores; 3) synthesize and export 24-nucleotide phased small interfering RNAs (phasiRNAs) to the meiocytes (Zhou et al., 2022); 4) synthesizes and supply lipophilic wax precursors to the epidermis and chloroplast lipids to the endothecium (Zhang et al., 2018; Zhu et al., 2020); 5)

synthesize and release exine components deposited onto the pollen grains; 6) provide an adhesive layer upon which the maturing pollen grains attach within the anther locule. Furthermore, a recent analysis in *Arabidopsis* discovered that tapetal cells also produced small interfering RNAs (siRNAs) which define the paternal methylome (Long et al., 2021). Associated with these sequential roles are considerable changes in tapetal anatomy and cellular constituents. Similar to pre-meiotic archesporial cells differentiating into meiotically competent pollen mother cells and then haploid gametophytes with major transcriptome changes accompanying specific transitions, Nan et al., 2022 hypothesized that the tapetum differentiates to match its various roles, but evidence of transcriptome reorganizations supporting such events has been lacking.

Our data clearly indicate several major reorganizations of the tapetal transcriptome (Fig. 4), similar to what is observed in the germinal lineage during the switch from mitosis to meiosis and again during haploid development. Specifically, we found suites of genes that are either completely activated or completely deactivated midway through meiosis (1.75–2.0 mm stages), corresponding with the transition from uninucleate to binucleate status, timing of phasiRNA production, and an overall increase in organelles. These transitional genes include known

male-sterility genes, such as *Ms44*, *Ms8*, *Zm3-3*, *Rf2*, and *bHLH122*, as well as a number of 24-PHAS loci, the precursors of 24-nt phasiRNAs, which accumulate during meiosis (Nan et al., 2022; Zhai et al., 2015). These data also provide examples of numerous unknown or unidentified genes that are differentially expressed over tapetal development, which could be potentially used as future marker genes or additional male-sterility genes (Suppl. Table 5). We conclude that tapetal cells do undergo major transcriptional changes to perform sequential, distinctive roles, acquiring the unusual feature of binucleation and later the morphology and function of secretory cells.

Little is known about the role of the middle layer beyond the fact that it degrades during meiosis - even that process is poorly understood. Considering the enrichment for the initial developmental stages in the early somatic cells cluster, it is likely that this cluster is composed of mitotically active SPL, middle layer, and tapetal cells that have not yet acquired specific identities based on gene expression. The somatic cells cluster also lacks any defining marker genes or biological function yet is enriched for cell cycle regulated genes, much like the early somatic cells, even though these genes were not used for clustering (Fig. 5). This lack of clear identity, alongside the enrichment for cell cycle-regulated genes suggests somatic anther cells largely lack defining transcriptional features or roles while dividing and instead most cease all division-related processes before committing to their cell-type function. Similarly, we hypothesize that the middle layer cells remain relatively undifferentiated, unlike their sister tapetal cells which clearly cluster together and are identified via known marker genes and functional roles.

The actual role of the middle layer in the anther has been hotly debated, as it is one of the most variable anther cell types across plant species. Even the number of middle layers can vary between plant taxa, as species in the family Hamamelidaceae can have two to three cell layers between the tapetum and endothecium when viewed transversely (Kubitzki et al., 2013). The unspecialized state of the middle layer supports the theory that this layer solely serves as a buffer between the endothecium and tapetum to prevent direct communication between these cell layers or to protect the tapetum from reactive oxygen species generated by the endothecium (Marchant and Walbot, 2022). Regardless, virtually no programmed cell death (PCD) transcripts were identified in either somatic or early somatic cell clusters, suggesting that the middle layer does not degrade via PCD, but rather is mechanically crushed by rapidly expanding tapetal cells.

The activation of photosynthesis in the endothecium is apparent in our developmental trajectory of this cell type, as suites of genes associated with photosynthesis are upregulated during and after meiosis. Other than those select genes, the endothecium is relatively static in its role and identity across anther development, confirming previous reports that it is one of the first anther somatic cell types to reach its final differentiated state. Unlike the other maize anther somatic cells, the endothecium continues to proliferate throughout anther elongation, beyond the 2.0 mm stage (Kelliher and Walbot, 2011), becoming an exception to the observation that cells attain differentiated status after the cessation of cell division.

The epidermis is the outermost protective cell layer of the anther. It is the first anther cell type to reach its final identity upon establishment of the anther primordia, differentiating from Layer1 (L1) cells in the meristem. We show that the epidermal transcriptome is almost completely static from inception to post-meiosis, with only minor changes in expression levels for particular genes. Wax and lipid biosynthesis genes were enriched in the epidermis relative to the other cell types, and these genes gradually increased expression within the epidermis across anther development.

The connective and vascular cells in-between the four anther lobes are completely unstudied and uncharacterized, despite their essential role of transporting water and nutrients from the rest of the plant to the lobes. We were able to readily identify a cluster of cells that met all the presumed biological features of the connective cells, as they were enriched for water transport, lignification, and various stimuli response

GO terms. These cells were largely uniform in expression patterns, varying little over the developmental series, yet clearly defined from the other cell types. Most vascular cells are dead or enucleated, with the maize anther containing only a small number of living phloem cells (<1% total cells), similar to the relative contribution of germinal cells. We therefore expected to identify phloem cells in the data. No vascular cells were identified via scRNA-seq in our dataset, although they are clearly released using the protocol (Marchant et al., 2022). These columnar cells exceed 50 μm in length, and so we hypothesize that they are removed by the filtration (40 μm sieve) step prior to cell isolation.

In summary, we established the developmental trajectories and timing of gene expression for functional roles for maize somatic cell types which house and support the developing germinal cells. We provide lists of putative marker genes for each cell type and potential new male-sterility genes, as well as the cell type specific expression patterns for known marker genes. The evolutionary conservation of transcription factors known to be essential for proper sporangia development in mosses, ferns, and flowering plants suggest these novel marker genes may be utilized for agricultural research spanning land plants (Fang et al., 2022; Lopez-Obando et al., 2022; Marchant and Walbot, 2022). This cell-level analysis will fuel future analyses of plant reproduction and male fertility.

4. Methods and materials

4.1. Plant growth and anther dissection

Zea mays (fertile inbred line W23 bz2) individuals were grown under greenhouse conditions in Stanford, CA, USA with 14-h day/10-h night lighting, approximating half of peak summer solar radiation including UV-A. Daily irrigation and fertilization maintained robust growth. Beginning five to six weeks after planting, individual plants were felled ~20 cm above ground level for sample collection between 8:00 and 9:00 a.m. The sacrificed stalk sections were taken to the lab within 10 min where the tassels were dissected out of the stem and leaf whorl. A Leica M60 dissecting scope (Leica Microsystems Inc.) and stage micrometer (Fisher Scientific) were used to isolate and measure anthers from the upper florets of spikelets along the central spike of the tassel.

4.2. Fixed cell isolation for scRNA-Seq

Anthers from individuals of W23 maize were dissected out. One of the three anthers per floret was used for imaging on a Nikon Diaphot inverted microscope with a Nikon D40 mounted camera at 10× magnification. The remaining two anthers per floret were fixed in ice-cold Farmer's solution (3:1100% ethanol: glacial acetic acid) for 2 h, washed twice for 5 min in 0.1X PBS, and then one anther was digested for 90 min at 50 °C in an RNase-depleted enzyme mix (Marchant et al., 2022) while the other anther was stored at –20 °C. Following digestion, shear force was applied to the anther between two microscope slides with thin tape on each end to prevent the anther from being fully crushed. The top microscope slide was slid back and forth 5–10 times, and the sample checked under the dissecting scope to ensure separation of the fixed cells. The cells were washed from the slides into 1 mL of cold 0.1X PBS via pipette and stained with 0.7 μL SYBR Green I nucleic acid gel stain (Invitrogen) for 20 min. The cells were then filtered through a 40 μm nylon cell strainer (Corning Inc.) into 50 mL Falcon tubes. The stained cells were then sorted into 96-well plates, each well containing 0.8 μL Primer Master Mix (0.225% Triton X-100, 1.6 mM dNTP mix, 1.875 μM barcoded oligo[dT] CEL-seq2 primers; Sigma-Aldrich, New England Biolabs) using a Hana Single Cell Dispenser (Namocell). Following cell sorting, the plates were spun at 400×g then stored at –80 °C. For each anther stage, at least two plates of 96 cells from two separate maize plants were prepared and sequenced.

4.3. CEL-Seq2 library preparation

Single-cell RNA-seq libraries were prepared following the CEL-Seq2 protocol (Hashimshony et al., 2016) with alterations similar to (Nelms and Walbot, 2019). The samples were thawed then incubated at 65 °C for 3 min, spun at 400×g, then incubated again at 65 °C for 3 min then placed on ice. To each sample 0.7 µL of reverse transcription mix (8:2:1:1 of Superscript IV 5X Buffer, 100 mM DTT, RNase Inhibitor, Superscript IV; ThermoFisher Scientific) was added, spun down, then incubated at 42 °C for 2 min, 50 °C for 15 min, 55 °C for 10 min then placed on ice. The samples were pooled by row into 8-strip tubes and excess primers were digested with the addition of 4.6 µL exonuclease I mix (2.5 µL of 10X Exonuclease I Buffer, 2.1 µL Exonuclease I; New England Biolabs) then incubated at 37 °C for 20 min, 80 °C for 10 min then placed on ice. To each of the pooled samples 44.28 µL (1.8X volume) of pre-warmed RNAClean XP beads was added and mixed well via pipette. The samples were left to incubate at RT for 15 min then placed on a magnetic rack until the liquid became clear. The supernatant was carefully pipetted out, making sure not to disturb the beads, and discarded. The beads were washed twice with 100 µL of freshly prepared 80% ethanol. The ethanol was pipetted out then the beads were left to dry for 5 min. The RNA was eluted from the beads with 7 µL RNase-free water and incubated for 2 min at RT then mixed via pipette.

Second strand synthesis was initiated with the addition of 3 µL s strand synthesis mix (2.31 µL Second Strand Reaction dNTP-free Buffer, 0.23 µL 10 mM dNTPs, 0.08 µL DNA ligase, 0.3 µL DNA polymerase I, 0.08 µL RNase H; New England Biolabs) and then incubated at 16 °C for 4 h. Samples were further pooled into a single tube and 30 µL Ampure XP beads (Beckman Coulter Life Sciences) with 66 µL bead binding buffer (2.5 M NaCl, 20% PEG 8000; Sigma-Aldrich) (1.2X volume) was added. The sample was incubated for 15 min at RT then washed and dried as described for the RNAClean XP beads above. The RNA was eluted from the beads with 6.4 µL of RNase-free water, left to incubate for 2 min at RT, and mixed via pipette.

In vitro transcription was initiated with the addition of 9.6 µL of MegaScript T7 IVT mix (1:1:1:1:1:1 of CTP solution, GTP solution, UTP solution, ATP solution, 10X Reaction Buffer, T7 Enzyme Mix; ThermoFisher Scientific) to the sample then incubated at 37 °C overnight. The beads were removed from the sample with a magnetic rack and 28.8 µL (1.8X volume) of pre-warmed RNAClean XP beads (Beckman Coulter Life Sciences) was added then incubated at RT for 15 min then washed and dried as described above. Once dry, 6.5 µL of RNase-free water was added to the beads, incubated for 2 min at RT, and mixed via pipette. The amplified RNA quality and quantity were analyzed with an RNA Pico 6000 chip on an Agilent 2100 BioAnalyzer (Agilent Technologies).

To the samples 1.5 µL of priming mix (9:5:1 of RNase-free water, 10 mM dNTPs, 1M tagged random hexamer primer: 5'-GCCTTGGCACCC-GAGAATTCCANNNNNN) was added and incubated at 65 °C for 5 min then placed on ice. A second round of reverse transcription was initiated with the addition of 4 µL of reverse transcription mix (4:2:1:1 of First Strand Buffer, 0.1 M DTT, RNaseOUT, SuperScript II; ThermoFisher Scientific) to each sample then incubated at 25 °C for 10 min, 42 °C for 1 h, and 70 °C for 10 min before being placed on ice. For the final PCR, 5.5 µL of sample were added to 21 µL of PCR master mix with Illumina TruSeq Small RNA PCR primer (RP1) and Index Adaptor (RPI "X") (6.5 µL RNase-free water, 12.5 µL Ultra II Q5 Master Mix, 1 µL of 10 µM RP1, 1 µL of 10 µM RPI "X"). Libraries were amplified with 13 rounds of PCR (98 °C for 30 s, then 13 cycles of 98 °C for 10 s, 65 °C for 15 s, and 72 °C for 30 s and finished with 72 °C for 3 min). The final PCR products were purified with 26.5 µL (1.0X volume) of Ampure XP beads (Beckman Coulter Life Sciences) then incubated at RT for 15 min then washed and dried as described above. The cDNA was eluted from the beads with 25 µL RNase-free water and purified again with 25 µL (1.0X volume) of Ampure XP beads (Beckman Coulter Life Sciences) then incubated at RT for 15 min then washed and dried as described above. The final purified libraries were eluted into 10 µL RNase-free water incubated for 2 min at

RT and mixed via pipette. The cDNA was then assessed with an Agilent BioAnalyzer High Sensitivity DNA chip.

The libraries were sequenced on a NovoSeq (Illumina) at Novogene Co. (Sacramento, CA, USA) with 150 base-pair (bp) paired-end reads. The 2.0 mm anther data from (Merchant et al., 2022) was also incorporated into our dataset. All primers were synthesized by the Stanford Protein and Nucleic Acid Facility (PAN, Stanford University, Stanford, CA, USA). Detailed step-by-step protocols of enzyme RNase-depletion, fixed cell isolation, and library preparation can be found in (Merchant et al., 2022).

4.4. Read filtering, mapping, and initial processing

Paired-end reads were processed similar to (Nelms and Walbot, 2019). Briefly, the raw reads were demultiplexed based on cell-specific barcodes (Suppl. Table 6) using Fastq-Multx (Aronesty, 2013). The UMI sequences from read 1 were added to the read 2 sequence names and then filtered and trimmed with Fastp (parameters: y -x -3 -f 6) (Chen et al., 2018). The clean reads were mapped to the B73 reference genome (AGP v. 4) (Jiao et al., 2017) with HiSat2 (Kim et al., 2019), and unique molecular identifiers (UMIs) quantified with SAMtools (Li et al., 2009) and UMI-tools (Smith et al., 2017).

To ensure we were capturing comparable transcript diversity to RNA-seq methods we compared the transcript diversity across all cells from 2.0 mm anthers in this study to that of whole anther RNA-seq analyses which were performed using the same library preparation and processing (Zhou et al., 2022).

Cell cycle heterogeneity has been shown to distort the clustering of cells, thus all cell cycle-regulated genes from (Nelms and Walbot, 2019) were removed. Cells with fewer than 250 UMIs or more than 100,000 UMIs were discarded. Genes that were detected in fewer than 3 cells were also discarded.

4.5. Cell clustering and cell type identification

All statistical analyses referenced in the text and figures and all plots were performed in R/RStudio (Team, 2015) with the following packages: ggplot2, dplyr, monocle3, ComplexHeatmap, ggpubr, seriation, prcurve, RSpectra. Cell clustering and cell type analyses were performed using Monocle 3 (Cao et al., 2019). The UMI counts for all cells were preprocessed using default parameters and their dimensionality reduced via Principal Component Analysis (PCA) consisting of 25 principal components based on the leveling point of the principal component variance plot. Batch effects from the multiple sequencing runs were removed with the "align_cds" function in Monocle and the clusters were determined and visualized with Uniform Manifold Approximation and Projection (UMAP) with a resolution of 0.001. The background information and quality metrics for each cell including anther stage, total number of UMIs, percentage of mitochondrial transcripts, percentage of plastid transcripts, and cluster can be found in Suppl. Table 7. The expression levels of known anther cell type marker genes (Suppl. Table 1) were mapped onto the UMAP and visualized for each cluster. Although cell cycle-regulated genes were not used in the clustering of the maize anther cells, the percentage of total transcripts mapped to cell-cycle regulated genes was independently calculated for each cell then further broken down into five stages of the cell cycle: G1, G1/S, S, G/M, and M (Nelms and Walbot, 2019).

Cluster-specific differentially expressed genes were identified and ranked using pseudo R² values from the "top_markers" and "marker-test_res" functions in Monocle. Default parameters were used with the exception of "fraction_expressing" which we increased to 0.2 from 0.1 ensuring that 20% or more of the cells within a cluster expressed the listed DE gene. Co-regulated genes were grouped into modules by using the "graph_test" function to calculate Moran's I for each gene then applying the Louvian community analysis with a resolution of 0.001 via the "find_gene_modules" function. We then plotted the aggregate

expression of all genes per module for each UMAP cluster to identify cluster-enriched gene modules (Suppl. Fig. 3). The genes from these cluster-enriched modules were then extracted and analyzed for gene ontology (GO) term enrichment relative to the Maize AGPv.4 reference in AgriGO v2 (Tian et al., 2017). The complete list of significantly enriched GO terms for each gene module can be found in Suppl. Table 3 and the co-regulated genes for each module in Suppl. Table 4.

4.6. Maize somatic cell type development

The calculations of pseudotime and pseudotime velocity were adapted from (Nelms and Walbot, 2022) and applied to the tapetum (uni- and binucleate), endothecium, epidermis, and connective cells. Briefly, the cells for each cell type were first ordered by anther stage, then within those stages ordered by gene expression patterns via pseudotime (Trapnell et al., 2014). The 2000 most variable genes for each cell type were used to calculate pseudotime as per (Nelms and Walbot, 2022). Pseudotime velocity calculates the rate of change in pseudotime for ordered cells, thus displaying rapid changes in gene expression as peaks. We visualized the expression patterns of the 50 most variable genes ordered by anther stage and pseudotime for each cell type. In addition, the expression levels of specific genes for each cell within the tapetum clusters were plotted relative to pseudotime.

CRediT authorship contribution statement

D. Blaine Merchant: Conceptualization, Data curation, Formal analysis, Funding acquisition, Investigation, Methodology, Visualization, Writing – original draft, Writing – review & editing. **Virginia Walbot:** Conceptualization, Funding acquisition, Investigation, Project administration, Resources, Supervision, Writing – review & editing.

Acknowledgments

This work was supported by the US National Science Foundation Plant Genome Research Program (NSF-PGRP) awards 1907220 (to D.B. M.) and 1754097 (to V.W.).

Appendix A. Supplementary data

Supplementary data to this article can be found online at <https://doi.org/10.1016/j.ydbio.2024.11.004>.

Data availability

Sequencing data are deposited in the NCBI Gene Expression Omnibus under accession GSE219091.

References

- Aronesty, E., 2013. Comparison of sequencing utility programs. *Open Bioinf. J.* 7, 1–8.
- Barnabás, B., Jäger, K., Fehér, A., 2008. The effect of drought and heat stress on reproductive processes in cereals. *Plant Cell Environ.* 31, 11–38. <https://doi.org/10.1111/j.1365-3040.2007.01727.x>.
- Cao, J., Spielmann, M., Qiu, X., Huang, X., Ibrahim, D.M., Hill, A.J., Zhang, F., Mundlos, S., Christiansen, L., Steemers, F.J., 2019. The single-cell transcriptional landscape of mammalian organogenesis. *Nature* 566, 496–502.
- Chen, S., Zhou, Y., Chen, Y., Gu, J., 2018. fastp: an ultra-fast all-in-one FASTQ preprocessor. *Bioinformatics* 34, i884–i890. <https://doi.org/10.1093/bioinformatics/bty560>.
- Cheng, P.C., Greysom, R.I., Walden, D.B., 1979. Comparison of anther development in genic male-sterile (*ms10*) and in male-fertile corn (*Zea mays*) from light microscopy and scanning electron microscopy. *Can. J. Bot.* 57, 578–596.
- De Strome, N., Geelen, D., 2014. The impact of environmental stress on male reproductive development in plants: biological processes and molecular mechanisms. *Plant Cell Environ.* 37, 1–18.
- Egger, R.L., Walbot, V., 2016. A framework for evaluating developmental defects at the cellular level: an example from ten maize anther mutants using morphological and molecular data. *Dev. Biol.* 419, 26–40. <https://doi.org/10.1016/j.ydbio.2016.03.016>.
- Egger, R.L., Walbot, V., 2015. Quantifying *Zea mays* L tassel development and correlation with anther developmental stages as a guide for experimental studies. *Maydica* 60, 1–5.
- Fang, Y., Qin, X., Liao, Q., Du, R., Luo, X., Zhou, Q., Li, Z., Chen, H., Jin, W., Yuan, Y., Sun, P., Zhang, R., Zhang, J., Wang, L., Cheng, S., Yang, X., Yan, Y., Zhang, X., Zhang, Z., Bai, S., Van de Peer, Y., Lucas, W.J., Huang, S., Yan, J., 2022. The genome of homosporous maidenhair fern sheds light on the euphylophyte evolution and defences. *Nat. Plants* 8, 1024–1037. <https://doi.org/10.1038/s41477-022-01222-x>.
- Fernández-Pérez, F., Vivar, T., Pomar, F., Pedreño, M.A., Novo-Uzal, E., 2015. Peroxidase 4 is involved in syringyl lignin formation in *Arabidopsis thaliana*. *J. Plant Physiol.* 175, 86–94.
- Fox, T., DeBruin, J., Haug Collet, K., Trimmell, M., Clapp, J., Leonard, A., Li, B., Sciaro, E., Collinson, S., Glassman, K., 2017. A single point mutation in *Ms44* results in dominant male sterility and improves nitrogen use efficiency in maize. *Plant Biotechnol. J.* 15, 942–952.
- Gómez, J.F., Talle, B., Wilson, Z.A., 2015. Anther and pollen development: a conserved developmental pathway. *J. Integr. Plant Biol.* 57, 876–891. <https://doi.org/10.1111/jipb.12425>.
- Hashimshony, T., Senderovich, N., Avital, G., Klochendler, A., de Leeuw, Y., Anavy, L., Gennert, D., Li, S., Livak, K.J., Rozenblatt-Rosen, O., 2016. CEL-Seq2: sensitive highly-multiplexed single-cell RNA-Seq. *Genome Biol.* 17, 77.
- Jiao, Y., Peluso, P., Shi, J., Liang, T., Stitzer, M.C., Wang, B., Campbell, M.S., Stein, J.C., Wei, X., Chin, C.-S., Guill, K., Regulski, M., Kumari, S., Olson, A., Gent, J., Schneider, K.L., Wolfgruber, T.K., May, M.R., Springer, N.M., Antoniou, E., McCombie, W.R., Presting, G.G., McMullen, M., Ross-Ibarra, J., Dawe, R.K., Hastie, A., Rank, D.R., Ware, D., 2017. Improved maize reference genome with single-molecule technologies. *Nature* 546, 524–527. <https://doi.org/10.1038/nature22971>.
- Jung, K.-H., Han, M.-J., Lee, D., Lee, Y.-S., Schreiber, L., Franke, R., Faust, A., Yephremov, A., Saedler, H., Kim, Y.-W., Hwang, I., An, G., 2006. *Wax-deficient anther1* is involved in cuticle and wax production in rice anther walls and is required for pollen development. *Plant Cell* 18, 3015–3032. <https://doi.org/10.1105/tpc.106.042044>.
- Kelliher, T., Egger, R.L., Zhang, H., Walbot, V., 2014. Unresolved issues in pre-meiotic anther development. *Front. Plant Sci.* 5, 1–9. <https://doi.org/10.3389/fpls.2014.00347>.
- Kelliher, T., Walbot, V., 2012. Hypoxia triggers meiotic fate acquisition in maize. *Science* 337, 345–348.
- Kelliher, T., Walbot, V., 2011. Emergence and patterning of the five cell types of the *Zea mays* anther locule. *Dev. Biol.* 350, 32–49. <https://doi.org/10.1016/j.ydbio.2010.11.005>.
- Kim, D., Paggi, J.M., Park, C., Bennett, C., Salzberg, S.L., 2019. Graph-based genome alignment and genotyping with HISAT2 and HISAT-genotype. *Nat. Biotechnol.* 37, 907–915.
- Kubitzki, K., Rohwer, J.G., Bittrich, V. (Eds.), 2013. Flowering Plants- Dicotyledons: Magnoliid, Hamamelid and Caryophyllid Families. Springer Science & Business Media.
- Li, D.-D., Xue, J.-S., Zhu, J., Yang, Z.-N., 2017. Gene regulatory network for tapetum development in *Arabidopsis thaliana*. *Front. Plant Sci.* 8, 1559.
- Li, H., Handsaker, B., Wysoker, A., Fennell, T., Ruan, J., Homer, N., Marth, G., Abecasis, G., Durbin, R., 2009. The sequence alignment/map format and SAMtools. *Bioinformatics* 25, 2078–2079.
- Li, Yanlong, Ma, H., Wu, Y., Ma, Y., Yang, J., Li, Yawei, Yue, D., Zhang, R., Kong, J., Lindsey, K., 2024. Single-cell transcriptome atlas and regulatory dynamics in developing cotton anthers. *Adv. Sci.* 11, 2304017.
- Long, J., Walker, J., She, W., Aldridge, B., Gao, H., Deans, S., Vickers, M., Feng, X., 2021. Nurse cell-derived small RNAs define paternal epigenetic inheritance in *Arabidopsis*. *Science* 373, eabh0556, 1979.
- Lopez-Obando, M., Landberg, K., Sundberg, E., Thelander, M., 2022. Dependence on clade II bHLH transcription factors for nursing of haploid products by tapetal-like cells is conserved between moss sporangia and angiosperm anthers. *New Phytol.* 235, 718–731. <https://doi.org/10.1111/nph.17972>.
- Lu, L., Hou, Q., Wang, L., Zhang, T., Zhao, W., Yan, T., Zhao, L., Li, J., Wan, X., 2021. Genome-wide identification and characterization of polygalacturonase gene family in maize (*Zea mays* L.). *Int. J. Mol. Sci.* 22, 10722.
- Merchant, D.B., Nelms, B., Walbot, V., 2022. FX-Cell: quantitative cell release from fixed plant tissues for single-cell genomics. *bioRxiv* 2010–2021.
- Merchant, D.B., Walbot, V., 2022. Anther development—the long road to making pollen. *Plant Cell* koac287. <https://doi.org/10.1093/plcell/koac287>.
- Murphy, K.M., Egger, R.L., Walbot, V., 2015. Chloroplasts in anther endothecium of *Zea mays* (Poaceae). *Am. J. Bot.* 102, 1931–1937.
- Nan, G.-L., Teng, C., Fernandes, J., O'Connor, L., Meyers, B.C., Walbot, V., 2022. A cascade of bHLH-regulated pathways program maize anther development. *Plant Cell* 34, 1207–1225.
- Nan, G.L., Zhai, J., Arikit, S., Morrow, D., Fernandes, J., Mai, L., Nguyen, N., Meyers, B.C., Walbot, V., 2017. MS23, a master basic helix-loop-helix factor, regulates the specification and development of the tapetum in maize. *Development* 144, 163–172. <https://doi.org/10.1242/dev.140673>.
- Nelms, B., Walbot, V., 2022. Gametophyte genome activation occurs at pollen mitosis I in maize. *Science* 375, 424–429.
- Nelms, B., Walbot, V., 2019. Defining the developmental program leading to meiosis in maize. *Science* 364, 52–56. <https://doi.org/10.1126/science.aav6428>.
- Santiago, J.P., Sharkey, T.D., 2019. Pollen development at high temperature and role of carbon and nitrogen metabolites. *Plant Cell Environ.* 42, 2759–2775. <https://doi.org/10.1111/pce.13576>.

- Shi, C., Zhang, J., Wu, B., Joumi, R., Yu, C., Meyers, B.C., Liang, W., Fei, Q., 2022. Temperature-sensitive male sterility in rice determined by the roles of AGO1d in reproductive phasiRNA biogenesis and function. *New Phytol.* 236, 1529–1544.
- Shigeto, J., Itoh, Y., Hirao, S., Ohira, K., Fujita, K., Tsutsumi, Y., 2015. Simultaneously disrupting AtPrx2, AtPrx25 and AtPrx71 alters lignin content and structure in *Arabidopsis* stem. *J. Integr. Plant Biol.* 57, 349–356.
- Skibbe, D.S., Wang, X., Borsuk, L.A., Ashlock, D.A., Nettleton, D., Schnable, P.S., 2008. Floret-specific differences in gene expression and support for the hypothesis that tapetal degeneration of *Zea mays* L. occurs via programmed cell death. *J. Genetics Genomics* 35, 603–616. [https://doi.org/10.1016/S1673-8527\(08\)60081-8](https://doi.org/10.1016/S1673-8527(08)60081-8).
- Smith, T., Heger, A., Sudbery, I., 2017. UMI-tools: modeling sequencing errors in Unique Molecular Identifiers to improve quantification accuracy. *Genome Res.* 27, 491–499.
- Team, R.s, 2015. RStudio: Integrated Development for R. RStudio, Inc., Boston, MA. URL: <http://www.rstudio.com/42.84>.
- Tian, T., Liu, Y., Yan, H., You, Q., Yi, X., Du, Z., Xu, W., Su, Z., 2017. agriGO v2. 0: a GO analysis toolkit for the agricultural community, 2017 update. *Nucleic Acids Res.* 45, W122–W129.
- Trapnell, C., Cacchiarelli, D., Grimsby, J., Pokharel, P., Li, S., Morse, M., Lennon, N.J., Livak, K.J., Mikkelsen, T.S., Rinn, J.L., 2014. The dynamics and regulators of cell fate decisions are revealed by pseudotemporal ordering of single cells. *Nat. Biotechnol.* 32, 381–386.
- van der Linde, K., Walbot, V., 2019. Pre-meiotic anther development. *Curr. Top. Dev. Biol.* 131, 239–256.
- Verma, N., 2019. Transcriptional regulation of anther development in *Arabidopsis*. *Gene* 689, 202–209. <https://doi.org/10.1016/j.gene.2018.12.022>.
- Walbot, V., Egger, R.L., 2016. Pre-meiotic anther development: cell fate specification and differentiation. *Annu. Rev. Plant Biol.* 67, 365–395. <https://doi.org/10.1146/annurev-arplant-043015-111804>.
- Wang, C.-J.R., Nan, G.-L., Kelliher, T., Timofejeva, L., Vernoud, V., Golubovskaya, I.N., Harper, L., Egger, R., Walbot, V., Cande, W.Z., 2012. Maize multiple archesporial cells 1 (*mac1*), an ortholog of rice TDL1A, modulates cell proliferation and identity in early anther development. *Development* 139, 2594–2603.
- Wiese, A.J., Torutaeva, E., Honys, D., 2024. The transcription factors and pathways underpinning male reproductive development in *Arabidopsis*. *Front. Plant Sci.* 15, 1354418.
- Xu, Q., Yang, L., Kang, D., Ren, Z., Liu, Y., 2021. Maize MS2 encodes an ATP-binding cassette transporter that is essential for anther development. *Crop J.* 9, 1301–1308. <https://doi.org/10.1016/j.cj.2021.04.001>.
- Zhai, J., Zhang, H., Arikit, S., Huang, K., Nan, G.-L., Walbot, V., Meyers, B.C., 2015. Spatiotemporally dynamic, cell-type-dependent premeiotic and meiotic phasiRNAs in maize anthers. *Proc. Natl. Acad. Sci. U. S. A.* 112, 3146–3151.
- Zhang, L., Luo, H., Zhao, Y., Chen, X., Huang, Y., Yan, S., Li, S., Liu, M., Huang, W., Zhang, X., Jin, W., 2018. Maize *male sterile 33* encodes a putative glycerol-3-phosphate acyltransferase that mediates anther cuticle formation and microspore development. *BMC Plant Biol.* 18, 318. <https://doi.org/10.1186/s12870-018-1543-7>.
- Zhang, X., Hong, M., Wan, H., Luo, L., Yu, Z., Guo, R., 2019. Identification of key genes involved in embryo development and differential oil accumulation in two contrasting maize genotypes. *Genes* 10, 993.
- Zhou, X., Huang, K., Teng, C., Abdelgawad, A., Batish, M., Meyers, B.C., Walbot, V., 2022. 24-nt phasiRNAs move from tapetal to meiotic cells in maize anthers. *New Phytol.* 235. <https://doi.org/10.1111/nph.18167>.
- Zhu, T., Li, Z., An, X., Long, Y., Xue, X., Xie, K., Ma, B., Zhang, D., Guan, Y., Ni, C., Dong, Z., Hou, Q., Zhao, L., Wu, S., Li, J., Jin, W., Wan, X., 2020. Normal structure and function of endothecium chloroplasts maintained by *ZmMs33*-mediated lipid biosynthesis in tapetal cells are critical for anther development in maize. *Mol. Plant* 13, 1624–1643. <https://doi.org/10.1016/j.molp.2020.09.013>.